Accurate interferometric retardance measurements

Kent B. Rochford and C. M. Wang

A two-polarization Michelson interferometer with a low-retardance beam splitter and digital signal processing is used to measure the retardance of optical devices. Error analysis of the improved optical system and data processing shows that the measurement has an uncertainty of 0.039° for measurements of nominally 90° retarders. Retardance variations arising from coherent reflections in the retarder used for intercomparison add an uncertainty of from 0.005° to 0.03°, increasing the combined measurement uncertainty to as much as 0.049°.

Key words: Fresnel rhomb, interferometry, polarization, retardance measurement.

1. Introduction

A National Institute of Standards and Technology effort to develop an accurate and stable retardance artifact has necessitated the development of accurate measurement methods for optical retardance.[1,2] To ensure accuracy, we developed three different methods that could be tested independently through the measurement of prototype stable retarders. Two methods rely on polarimetric techniques, and one of these has been automated and adopted as our primary measurement tool. For our third measurement, we selected an interferometric technique that would exhibit different error sources and complement the polarimetric measurements.

Interferometric retardance measurements were first reported by Hazebroek and Holscher[3] and Hazebroek and Visser.[4] For our system, we made several modifications to this optical system: a specially designed low-retardance beam splitter was incorporated to reduce system biases, and digital filtering was implemented to quantify and to reduce data-processing errors. A very linear transducer was used to sweep the interferometer through its transfer function and to provide highly sinusoidal fringes that minimize measurement errors. We discuss the alignment and the operation of our interferometric system for measuring retardance, analyze the measurement error sources, and report our estimate of measurement accuracy.

2. Overview of Interferometric Retardance Measurements

The optical layout of our system is shown in Fig. 1. Our system is a two-polarization Michelson interferometer that allows two orthogonal linear polarizations to propagate over a common path that differs only inside the retarding device under test. We set the input polarization azimuth to bisect the retardance axes of the retarder. The axes of the output polarizing beam splitter (PBS) are carefully aligned to coincide with the retarder axes so that the principal polarization states of the system correspond to the retarder's axes.

For an ideal Michelson interferometer, transmittance $T = \frac{1}{2}[1 + \cos(\Delta\phi)]$, where $\Delta\phi$ is the phase difference between the two arms of the interferometer. Driving the piezoelectric actuator (see Fig. 1) to produce a linear phase change yields two orthogonally polarized sinusoidal output intensities. Retardance δ_0, however, causes the two linear polarizations in the interferometer to have a fixed path difference $2\delta_0$ from two passes through the retarder. Thus the two detected signals exhibit a $2\delta_0$ phase difference.

As the piezoelectric transducer is driven with a ramped voltage, N samples are acquired over many periods of the detected sinusoids. The phase difference between each waveform is calculated with software that converts the acquired data sets $s_{1,2}(t_i)$ into two phasor time series $z_{1,2}(t_i) = A_{1,2}(t_i) \cos[\phi_{1,2}(t_i)]$. The instantaneous phase difference between the two data sets is taken at each time, and the average phase

The authors are with the National Institute of Standards and Technology, 325 Broadway, Boulder, Colorado 80303-3328. K. B. Rochford and C. W. Wang are in the Optoelectronics Division and the Statistical Engineering Division, respectively.

Received 8 October 1996; revised manuscript received 5 February 1997.

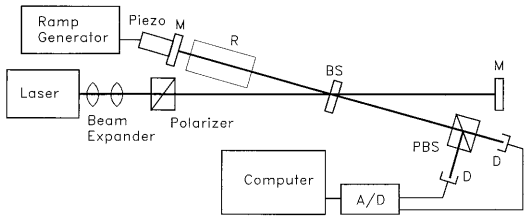

Fig. 1. Experimental layout for interferometric retardance measurement. Components include mirror, M; beam splitter, BS; polarizing beam splitter, PBS; retarder, R; analog-to-digital converter, AID; two detectors, D.

difference $\langle\phi\rangle$ is calculated over the N time points with

$$\langle\phi\rangle = \frac{1}{N}\sum_{i=1}^{N}[\phi_1(t_i) - \phi_2(t_i)]. \tag{1}$$

This conversion of real data to phasor data is performed with the Hilbert transform to form a complex analytic signal.[5] For a real function $s(t)$, we assume the existence of a complex function $z'(t) = s(t) + is_H(t)$, where $s_{\mathrm{H}}(t)$ is the Hilbert transform of $s(t)$ (see Ref. 6). The phasor form $z(t)$ is found easily from $z'(t)$ because $A(t) = [s(t)^2 + s_{\mathrm{H}}(t)^2]^{1/2}$ and $\phi(t) = \tan^{-1}[s_{\mathrm{H}}(t)/s(t)]$.

To find the analytic signal from real data, we note that the Fourier transform of $s_{\mathrm{H}}(t)$ is

$$\mathcal{F}[s_{\mathrm{H}}(t)] = -iS(f)\mathrm{sgn}(f), \tag{2}$$

where $S(f)$ is the Fourier transform of $s(t)$, and the sign function $\mathrm{sgn}(f)$ yields -1 for $f < 0$ and $+1$ for $f > 0$. Using this result to find the Fourier transform of $z'(t)$, we obtain

$$\begin{aligned}\mathcal{F}[z'(t)] &= 0 \qquad f < 0\\ &= 2S(f) \quad f > 0\end{aligned} \tag{3}$$

so that $z'(t) = \mathcal{F}^{-1}[2S_+(f)]$, where $S_+(f)$ is the single-sided Fourier transform (that is, all negative coefficients set to zero) of $s(t)$.

This method is used to convert real data sets $s_{1,2}(t)$ into an array of instantaneous phases $\phi_{1,2}(t)$ with fast Fourier transforms (FFT's) in software. First, we take the FFT of both data sets and set the coefficients for frequencies $f \leq 0$ to zero. Then we perform the inverse FFT on both data sets to obtain complex data sets $z_{1,2}'(t)$ and calculate the phase at each point using $\phi_{1,2}(t_i) = \tan^{-1}[s_{\mathrm{H};1,2}(t_i)/s_{1,2}(t_i)]$. The average phase is found with Eq. (1) and the measured retardance $\delta_m = \langle\phi\rangle/2$.

3. System Considerations

A. Optical System

The importance of properly aligning the retarder and the polarization axes is shown by modeling the system with Jones calculus. For an input polarizer with a transmission axis at angle α, an output polarizer at β, and the retardance axes at γ with respect to vertical, the measured retardance δ_m is

$$\delta_m = \tan^{-1}\left[\tan\left(\frac{\delta_0}{2}\right)F_1\right] - \tan^{-1}\left[\tan\left(\frac{\delta_0}{2}\right)F_2\right], \tag{4}$$

where δ_0 is the true retardance and

$$F_{1,2} = \frac{\cos(2\alpha - 2\gamma) \pm \cos(2\beta - 2\gamma)}{1 \pm \cos(2\beta - 2\alpha)}. \tag{5}$$

Equation (4) shows that $\delta_m = \delta_0$ when $F_1 = 1$ and $F_2 = -1$. These conditions are met for all angles α when $\beta = \gamma$ (the retarder and the output polarizer axes are exactly coincident). Experimentally, α determines the amplitude of signals $s_{1,2}(t)$, and $\alpha = 45 \pm 1°$ was used so both detected signals had approximately equal magnitudes.

In principle, we can find δ_0 by measuring retardance δ_m *versus* the output polarizer angle β for several input polarizer angles α. The point where curves of retardance *versus* β intersect for two or more different angles α occurs when $\beta = \gamma$ or when the retarder and the output polarizer axes are aligned. Because this process is time consuming, we polarimetrically aligned the retarder and the output polarizer axes. The beam was normally incident upon the retarder, and we ensured this by monitoring the backreflection of a 633-nm He–Ne laser that was aligned along the IR beam path.

We used a Glan–Thompson polarizer at the input and a Glan air-spaced PBS as the output polarizer. The extinction ϵ for the undeviated transmitted beam was 4×10^{-6}, allowing a minimum resolvable nulling angle of $\theta_{\min} = \sin^{-1}(\epsilon^{1/2}) \approx 0.1°$; thus the retarder axes could be aligned polarimetrically within $\pm 0.1°$. The reflected polarization at the analyzer exits at an angle very close to an orthogonally polarized ghost reflection, so a second polarizer was added to block the undesirable reflection and to improve the extinction to $\epsilon = 10^{-4}$. InGaAs photodiodes and transimpedance amplifiers detected the reflected and the transmitted beams from the analyzer.

Our measurements were made with a three-mode, single-line, diode-pumped Nd:YAG laser at 1.319 μm. A simple two-lens afocal telescope provided a 2-mm diameter collimated beam. The planar mirrors and the beam splitter were aligned so that a single, nonlocalized circular interference pattern exited the interferometer. When this maximum-visibility single fringe results, mirror tilts are minimized and beams are normally incident upon the mirrors.

Aluminum mirrors contribute 180° retardance when the beam is normally incident, and this has no effect on retardance measurements. For nonnormal incidence, metallic mirrors impart a retardance δ_{Al} given by[7]

$$\tan(\delta_{\mathrm{Al}}) = \frac{2n\kappa\sin(\theta)\tan(\theta)}{n^2(\kappa^2 + 1) - \sin^2(\theta)\tan^2(\theta)}, \tag{6}$$

where θ is the angle of incidence, the refractive index $n \approx 1.3$, and the extinction coefficient $\kappa \approx 13$ for aluminum at 1.3 μm (see Ref. 8). The retardance change is $<0.01°$ for $\theta < 2.1°$. By monitoring back-reflections of the interferometer beams during alignment, we ensure that the mirrors have a net tilt of less than 0.1°, so retardance is negligible.

Apart from the retarder being measured, the only element that adds significant retardance is the beam splitter. Ideal beam splitters exhibit phase reversibility[9] (i.e., beams incident upon both sides of the beam splitter see the same retardance); if not reversible, the interferometer will measure the beam-splitter retardance as well. Measurements of commercial cube beam splitters showed net retardance differences of more than 40° when reflections from both beam splitter faces were compared. Though this could be subtracted from retardance measurements, we considered this undesirable because a large beam-splitter retardance would also show variation with input angle and position greater than an initially small retardance.

To minimize such error, we used a beam splitter designed for minimal retardance at each reflection so that the retardance difference between opposite reflections would be as small as possible. Retardance occurs when light is incident upon dielectric layers because the s and p polarizations have different Fresnel coefficients and the sum of reflected amplitudes combines algebraically (owing to the optical path of each film layer) to yield a phase difference between polarizations. This retardance can be eliminated if the beam is normally incident (so the Fresnel coefficients are equal) or if the dielectric layers have quarter-wave optical thickness. We used a 50/50 beam splitter for 6° incidence fabricated with only quarter-wave layers. The film was deposited onto a low stress-optic glass[2] so that substrate retardance was negligible. An antireflection coating with quarter-wave layers was deposited on the opposite side of the substrate to minimize errors from multiple reflections.

Path matching and collimation are important for maximizing fringe visibility and ensuring that the interfering wave fronts have similar curvature. A superluminescent diode aligned along the Nd:YAG beam was used to path match the interferometer arms within <10 μm. Even with well-matched paths, circular fringes can result owing to spherical and other aberrations caused by the beam-splitter plate. Adjustment of the collimating telescope to produce beams that were clearly converging or diverging caused retardance changes of up to $\pm 0.1°$. This might be because of the angle sensitivity of beam-splitter retardance, the appearance of retardance at the mirrors at nonnormal incidence, and the angle sensitivity of polarizer extinction. To minimize these effects, we carefully collimated the beam and placed a 2-mm-diameter aperture just before the output polarizer to block fringes beyond the main lobe.

B. Electronic and Signal Processing Considerations

To obtain sinusoidal waveforms from the interferometer, we drive a linearized piezoelectric transducer with a triangular voltage waveform. During the positive slope of the driving voltage, well away from the nonlinear turning points, the analog-to-digital converter with simultaneous sample and hold acquires $N = 8192$ samples at 330 kHz. The slope of the driving voltage is adjusted so that the transducer travels 12.53 μm (19 fringes) during the data-acquisition window. Because the data are taken quickly ($\approx$25 ms), low-frequency vibrations have little effect on the interferometric data. Furthermore, because the two optical paths we compare propagate over the same physical path, phase shifts resulting from temperature, vibration, air currents, and so forth, are common mode and cancel when the retardance phase difference is calculated [see Eq. (1)].

The piezoelectric positioner used capacitive sensing and feedback control to ensure linearity. We analyzed a typical data set statistically, using complex demodulation techniques to obtain phase and amplitude residuals that result when the waveform is compared with that expected from an ideal system. The phase showed a slowly varying deviation from linearity with a maximum variation of $\pm 14°$ over the $\approx 19 \times 360°$ displacement. The amplitude residual showed random variations with a standard deviation of 0.06% of the mean peak-to-peak amplitude; this corresponds to both noise and drift in the optical source and to the detection, amplification, and signal acquisition process.

Because FFT's are applied to the data, the data sets should contain an integral number of cycles of data, otherwise spectral artifacts will arise from discontinuities at the data end points.[10] Positioner translation was adjusted to obtain data sets that were within $\pm 12°$ of 19 fringes ($19 \times 360° \pm 12°$). To further mitigate errors from spectral artifacts, the time series data $s_{1,2}(t)$ were multiplied by a Hanning window $[\cos^2(x)]$ to attenuate end-point effects before performing FFT's. Finally, the first and last 499 data points were dropped when the average retardance was calculated, so we actually calculated retardance by summing over $i = 500$ to $8192 - 500$ in Eq. (1). These steps allowed us to eliminate errors that arose as the data were forced to be artificially periodic by the FFT processing.

Obtaining a single retardance measurement, including data acquisition and FFT's, required $\sim$5 s with a 33 MHz 486-type computer system. Typically, 50–200 measurements were made and the mean and standard deviation were calculated.

4. Error Sources in Retardance Measurement

We identified several possible error sources that contribute to measurement uncertainty. In this section we discuss errors that arise from optical-system misalignments and imperfections, phase-calculation limitations, and retarder imperfections. The standard

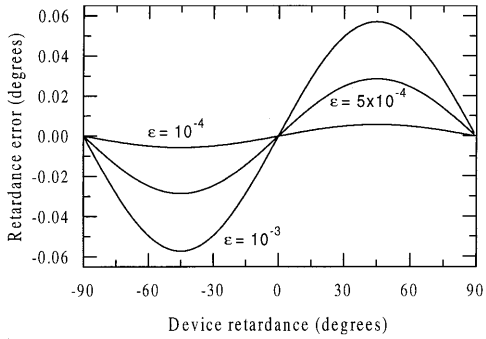

Fig. 2. Retardance error resulting from finite polarizer extinction ϵ.

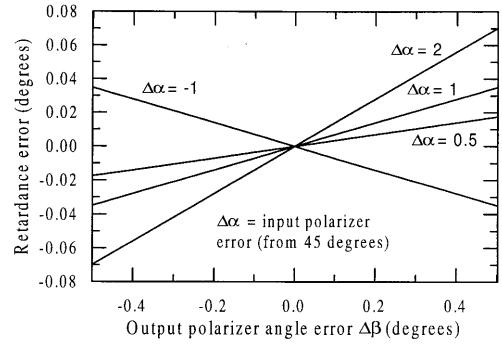

Fig. 3. Retardance error arising from polarizer misalignment $\Delta\alpha$ and $\Delta\beta$.

uncertainty u (estimated standard deviation) that arises from each error source is given below.

A. Polarizer Extinction

Because the reflected polarization from the analyzer has an extinction of $\epsilon = 10^{-4}$, a small amount of the orthogonal polarization leaks into the detected beam. To estimate the error induced by this leakage, we assume the detected signal is the sum of the desired signal $s_1(t)$, which has phase δ_0, and a fraction ϵ of the undesired signal $s_2(t)$ that has phase $-\delta_0$. Thus the detected signal from the reflected beam has the form $s(t) \approx \cos(\omega t + \delta_0) + \epsilon \cos(\omega t - \delta_0)$, and the phase of this combined signal is

$$\phi_{\mathrm{PE}} = \tan^{-1}\left[\frac{\sin(\delta_0) + \epsilon \sin(-\delta_0)}{\cos(\delta_0) + \epsilon \cos(-\delta_0)}\right]. \tag{7}$$

The phase error due to polarizer leakage $\Delta\delta_{\mathrm{PE}}$ equals $\delta_0 - \phi_{\mathrm{PE}}$ and is plotted for several polarizer extinctions in Fig. 2. The figure shows that high-extinction polarizers are not required for these measurements. For a retarder with $\delta_0 = 89.4°$ and $\epsilon = 10^{-4}$, $\Delta\delta_{\mathrm{PE}} = 1.2 \times 10^{-4}$ deg, and the retardance uncertainty resulting from polarizer extinction $u_R = \Delta\delta_{\mathrm{PE}}$.

B. Retarder–Polarizer Alignment

The error resulting from retarder–polarizer misalignment $\Delta\delta_{\mathrm{PA}}$ equals $\delta_0 - \delta_m$, where δ_m is calculated from Eq. 4. The error is zero when $\beta = \gamma = 0°$. Figure 3 shows the retardance errors expected from polarizers with angle errors $\Delta\alpha$ and $\Delta\beta$ for $\delta_0 = 90°$. Maximum uncertainty in retardance for our experimental angle uncertainties $\Delta\alpha_{\max} = \pm 1°$ and $\Delta\beta_{\max} = \pm 0.1°$ is $\Delta\delta_{\mathrm{PA}} = \pm 4 \times 10^{-4}$ deg for a retardance of 89.4°. Because this is a worst-case estimate of a normally distributed error, the retardance uncertainty for polarizer misalignment is $u_{\mathrm{PA}} = \Delta\delta_{\mathrm{PA}}/3 = 1 \times 10^{-4}$ deg.[11]

C. Beam Collimation

We estimated the effect of beam collimation on retardance empirically by changing the spacing of the two telescope lenses to produce obvious divergence or convergence. A maximum retardance change $\Delta\delta_{\mathrm{BC}} = 0.08°$ was observed. Since this is a worst-case estimate, the retardance uncertainty $u_{\mathrm{BC}} = \Delta\delta_{\mathrm{BC}}/3 = 0.027°$.

D. Beam-Splitter Retardance

Thirty measurements of the system with no retarder in place yielded a mean beam-splitter retardance of $\delta_{\mathrm{B}} = -0.020°$ with a standard deviation of 0.028°. This standard deviation is a measure of the repeatability of the system, so the uncertainty $u_{\mathrm{B}} = 0.028°$.

E. Combined Uncertainty from Measurement System Errors

We estimated measurement system errors by combining the uncertainties above using the root sum of squares. The resulting uncertainty for our system $u_{\mathrm{S}} = (u_{\mathrm{R}}^2 + u_{\mathrm{PA}}^2 + u_{\mathrm{BC}}^2 + u_{\mathrm{B}}^2)^{1/2} = 0.039$, and it is dominated by factors that directly alter retardance in the system: the beam splitter and the effect of beam divergence or convergence. Uncertainty from alignment errors is negligible, but this is partially due to errors that decrease for retardances near 90°. We can correct the retardance bias introduced by the beam-splitter retardance by subtracting the mean value δ_{B} from the measured value, so that the estimated retardance $\delta = \delta_m + 0.02°$.

5. Phase Calculation Uncertainty

The phase was calculated using FFT's instead of analog instrumentation such as a vector voltmeter or lock-in amplifier because the calculation error could be estimated with simulated data that incorporated estimates of noise and other imperfections. Furthermore, the error estimate would be stable as long as the noise or imperfections of acquired data stayed within specified limits.

We performed Monte Carlo simulations to estimate the errors that arose from the FFT processing of typical data sets. Pairs of data sets with a known phase difference, and which incorporated the estimated values for amplitude noise, slowly varying phase error, nonperiodicity, and so forth (Subsection 3.B) were formed and processed. Calculation errors were determined as the phase shift calculated from the FFT processing was compared with the preset phase shift for 50 trials with simulated data.

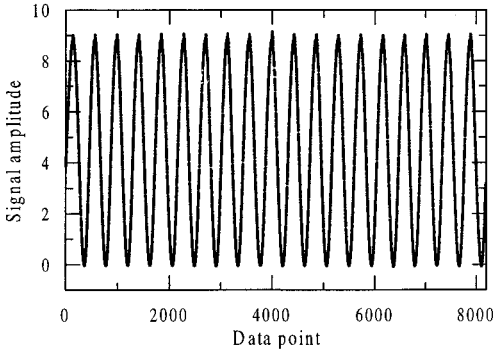

Fig. 4. Typical fringe data from interferometer.

For simulated data sets similar to our typical data shown in Fig. 4 [Gaussian amplitude noise with standard deviation $\sigma_A = 0.08\%$, 13° overshoot (18.96 periods in a data set), and slow phase modulation], the calculated values varied as much as ±0.11° around the true value. For 50 trials, the mean calculated retardance was 3×10^{-4} deg smaller than the true value, and the standard deviation $\sigma = 6 \times 10^{-3}$ deg. If 50 measurements are taken with similar noise in the data, the standard retardance uncertainty $u_P = \sigma/\sqrt{50} \approx 8 \times 10^{-4}$ deg.

The processing is tolerant of amplitude noise; simulations with 5 times more amplitude noise ($\sigma_A = 4\%$) yields an error of 6×10^{-4} deg from the true value and a standard deviation $\sigma = 0.025°$. Repeating this simulation with the slowly varying phase error replaced with Gaussian phase noise ($\sigma_P = 15°$) increased the standard deviation of the calculated values to 0.033°; even with these greatly overestimated noise values, an uncertainty of $<5 \times 10^{-3}$ deg can be obtained as 50 measurements are averaged. Because our data acquisition is automated, we routinely take 50 or more measurements to make one independent retardance estimate. Thus the errors associated with processing noisy, nonperiodic data are negligible compared with the optical-system uncertainty $u_S = 0.039°$ discussed above.

6. Uncertainty Arising from Retarder

We fabricated a double-rhomb retarder that is stable with temperature, input angle, and wavelength and thus provided an excellent means for comparing this measurement method with others.[1,2] Five devices were fabricated and measured, and the results were compared with those made with two different polarimetric systems.[12,13] to demonstrate the accuracy of our measurements. Because the intercomparisons are affected by retardance uncertainties in the devices, device uncertainties must be estimated.

A. Coherent Reflections

The largest uncertainty arises from the reflectance of the rhomb faces. Because the laser used in this measurement has a long coherence length, multiple reflections can interfere coherently and cause variations in the device retardance. The double-rhomb retarder has AR-coated end faces with reflectance R_1 and an internal interface coated to provide reflectance R_2; thus retardance variation arises from multiple reflections between the end faces and between the internal interface and the end faces. The resulting retardance is a complicated function of reflectances, design retardance (i.e., that due to total internal reflections in the rhombs), and optical path length. If we assume the optical path length varies uniformly over $[0, 2\pi]$ over a series of measurements, the device retardance can be described by a probability density function. For a nominal 90° retarder, the retardance variation has zero mean and standard deviation $\sigma_R \approx [2(R_1{}^2 + R_1R_2)]^{1/2}$ (see Ref. 2). For our stable retarder, a temperature change of 0.3 °C is sufficient to change the optical path by 2π; thus averaging repeated measurements made over a reasonable period yields the true retardance.

Our device is designed to have antireflection coatings so that R_1, <0.001, $R_2 < 0.0005$, and the maximum retardance variation is ±0.17° (see Ref. 2). Some coatings on early prototypes used in the evaluation of our measurement accuracy had higher reflectance. The effect of multiple coherent reflections is seen in Table 1, which lists the predicted (σ_R) and measured (σ_m) standard deviation of several retardance measurements for m independent measurements. As expected, the measured standard deviation is less than the predicted value because the interfering beams are not fully coherent.

Table 1. Worst-Case and Measured Variation Caused by Coherent Reflections

Device	R_1	R_2	σ_R (deg)	σ_m (deg)	m	$u_R = \sigma_m/\sqrt{m}$ (deg)
SR1	0.002	0.001	0.20	0.02	19	5×10^{-3}
SR2	0.008	0.001	0.69	0.09	9	0.03
SR3	0.008	0.001	0.69	0.12	15	0.03
SR4	0.001	<0.001	0.12	0.06	11	0.02
SR5	0.001	<0.001	0.12	0.06	10	0.02

B. Input Angle

Equation (2) of Ref. 2 gives the retardance uncertainty due to error Γ_i of the input angle from normal incidence. We estimate the maximum Γ_i by assuming that the rhomb can be aligned using backreflection of a visible laser beam (coaligned with the infrared beam) with a resolution of 1 beam diameter. For a nominal path of 50 cm, and a maximum beam diameter of 2 mm, the maximum input angle uncertainty $\Gamma_{max} = \tan^{-1}(2/500) = 0.23°$. The acute angles α_R for the five rhombs varied between 76.3° and 76.4°, so the corresponding retardance error resulting from input angle error Γ_{max} was less than 2×10^{-4} deg for all measurements. This represents a worst-case error, and the standard uncertainty $u_\Gamma = \Gamma_{max}/3 < 1 \times 10^{-4}$ deg. Both positive values and negative values of input angle Γ decrease the retardance of the rhomb.

Table 2. Uncertainty Caused by Twist in Rhomb

	SR1	SR2	SR3	SR4	SR5
ϵ_t (deg)	0.36	0.24	0.6	0.72	0.2
$\Delta\beta_T$ (deg)	0.18	0.12	0.3	0.36	0.1
$u_{PA/T}$ (deg)	2.2×10^{-3}	1.0×10^{-3}	6.3×10^{-3}	8.9×10^{-3}	6.9×10^{-4}

C. Rhomb Assembly

The retarder is made by attaching two rhombs with retardance $\delta_0/2$. During the alignment it is possible to include a small rotation, or twist ϵ_t, between the devices. Twist causes an alignment error $\Delta\beta_T = \frac{1}{2}\epsilon_t$ because the nulling angle that occurs between crossed polarizers is found with less resolution. (We conservatively assign this error to the analyzer angle $\Delta\beta$ instead of the less sensitive polarizer error $\Delta\alpha$.) Retardance error resulting from this misalignment $u_{PA/T} = \delta_0 - \delta_m$, where δ_m is calculated from Eq. (4) with $\alpha = 45°$, $\gamma = 0°$, and $\beta = \Delta\beta_T = \frac{1}{2}\epsilon_t$. This value is generally different from the error $u_{PA} = \pm 1 \times 10^{-4}$ because of polarizer and analyzer alignment errors $\Delta\alpha$ and $\Delta\beta$. The resulting retardance errors $u_{PA/T}$ are tabulated in Table 2.

For all rhombs measured, $\Delta\beta_T$ is greater than the $\pm 0.1°$ error with which we can otherwise locate the retarder axes. As a result, the measurement errors $u_{PA/T}$ arising from twist are greater than those arising from axis determination. This error affects the combined uncertainty from measurement system errors calculated above, and the combined system uncertainty u_s can be recalculated with this higher value of $u_{PA/T}$ in place of u_{PA}. Thus u_S depends on the retarder characteristics and increases by up to 0.001° to $u_S = 0.040°$.

7. Combined Measurement Uncertainty

The uncertainty caused by multiple reflections u_R clearly dominates the uncertainties arising from the retarder. This can be combined with the system uncertainty u_S to form the measurement uncertainty $u_c = (u_S^2 + u_R^2)^{1/2}$. The retardance δ and the uncertainties for the five measured devices are shown in Table 3. The expanded uncertainty U uses a coverage factor of 2 so that the true value is within $\delta \pm U$ approximately 95% of the time.[11]

As Table 3 shows, the retardance variation resulting from coherent interference significantly increases the measurement uncertainty. As discussed before, we can decrease this somewhat by increasing the number of measurements in devices that undergo path changes of $\lambda/2$ over modest temperature changes. For thin devices this approach might not work unless device reflectance is sufficiently low or the source coherence is decreased.

Table 3. Retardance Measurements and Measurement Uncertainty

Device	δ (deg)	u_S (deg)	u_R (deg)	u_c (deg)	$U = 2u_c$ (deg)
SR1	89.21	0.039	0.005	0.039	0.078
SR2	89.38	0.039	0.03	0.049	0.098
SR3	89.46	0.039	0.03	0.049	0.098
SR4	87.79	0.040	0.02	0.045	0.090
SR5	89.32	0.040	0.02	0.045	0.090

8. Estimate of Accuracy

Measurements made with this system were compared with measurements made with two different polarimetric systems as part of our effort to determine overall measurement accuracy.[2,12,13] Each of the stable rhomb retarders was measured on each system and the retardance values were compared. This intercomparison shows that the interferometric retardance measurements are accurate to within the stated uncertainty.[2] This confirms that our error analysis neither underestimated nor overlooked any important error sources.

9. Conclusions

We demonstrate a system for interferometric retardance measurements with a standard uncertainty $u = 0.04°$. Integral to this result were the implementation of a low-retardance beam-splitter element, a linear driving transducer that provides sinusoidal output signals, and digital signal processing that adds negligible (and quantifiable) error. Coherent reflections can alter the effective retardance and increased uncertainty to $u_c = 0.049°$ for our devices. If the sample is sufficiently thick so that the optical path can change by $\lambda/2$ over modest temperature variations, repeated measurement of the retarder can reduce the error associated with coherent reflections.

We thank Dominic Vecchia for assistance with the complex demodulation analysis and Paul Hale for helpful discussions regarding the experimental apparatus.

References

1. K. B. Rochford, P. A. Williams, A. H. Rose, I. G. Clarke, P. D. Hale, and G. W. Day, "Standard polarization components: progress toward an optical retardance standard," in *Polarization Analysis and Measurement II*, D. H. Goldstein and D. B. Chenault, eds., Proc. SPIE **2265,** 2–8 (1994).
2. K. B. Rochford, A. H. Rose, P. A. Williams, C. M. Wang, I. G. Clarke, P. D. Hale, and G. W. Day, "Design and performance of a stable linear retarder," Appl. Opt. **36,** 6458–6465 (1997).
3. H. F. Hazebroek and A. A. Holscher, "Interferometric ellipsometry," J. Phys. E **6,** 822–826 (1973).
4. H. F. Hazebroek and W. M. Visser, "Automated laser interferometric ellipsometry and precision reflectometry," J. Phys. E **16,** 654–661 (1983).
5. D. Gabor, "Theory of communication. Part I. The analysis of information," J. Inst. Elec. Eng. **93,** 429–441 (1946).

6. R. N. Bracewell, *The Fourier Transform and Its Applications* (McGraw–Hill, New York, 1986), pp. 267–271.
7. M. Born and E. Wolf, *Principles of Optics* (Pergamon, Oxford, 1980), Vol. 6, pp. 619.
8. R. A. Paquin, "Properties of metals," in *Handbook of Optics*, M. Bass, E. W. Van Stryland, D. R. Williams, and W. L. Wolfe, eds. (McGraw-Hill, New York, 1995), Vol. 2 p. 35.22.
9. A. L. Fymat, "Jones' matrix representation of optical instruments. I: Beam splitters," Appl. Opt. **10,** 2499–2505 (1971).
10. F. J. Harris, "On the use of windows for harmonic analysis with discrete Fourier transform," Proc. IEEE **6,** 51–83 (1978).
11. B. N. Taylor and C. E. Kuyatt, *Guidelines for evaluating and expressing the uncertainty of NIST measurements* National Institute of Standards Technology Technical Note 1297, 1993 (U.S. Government Printing Office, Washington, D.C.), pp. 2–5.
12. P. A. Williams, A. H. Rose, and C. M. Wang, "Rotating-polarizer polarimeter for accurate retardance measurement," Appl. Opt. **36,** 6466–6472 (1997).
13. K. B. Rochford and C. M. Wang, "Uncertainty in null polarimeter measurements," IR. 5055, 1996 (National Institute of Standards and Technology, Gaithersburg, Md.).
14. E. Hecht and A. Zajak, *Optics* (Addison–Wesley, Reading, Mass, 1974), pp. 301–305.